THE CORONAL CONDENSATION OBSERVED AT THE 1973 ECLIPSE

1973年日食におけるコロナルコンデンセーション

黒河宏企

主論文

THE CORONAL CONDENSATION OBSERVED AT THE 1973 ECLIPSE

HIROKI KUROKAWA

Kwasan Observatory, University of Kyoto,

Yamashina, Kyoto, Japan

Abstract. The flash spectrograms obtained at the June 30, 1973 eclipse contain the monochromatic images of a coronal condensation in three coronal lines of FeXIV 5303, FeX 6374 and FeXI 7892 and Hα line. The assumption of the axially-symmetric distribution of the emissivity in the coronal lines allows us to find the density and temperature structure of the coronal condensation. While the electron density in the central axis of the condensation is about ten times as high as that of the normal corona at each height, the temperature is not so high ($T \leqslant 2.3 \times 10^6$ K). This seems to be a representative nature of a coronal active region in the post maximum phase of activity. It is found that there exists a cool and dense core ($T = 10^6$ K, $Ne = 6 \times 10^9$ cm^{-3} at 17000 km) at the lower part of the coronal condensation, which is in a close geometrical coincidence with the small active prominence protruding from the underlying plage region.

1 Introduction

The difficulties in determining the thermodynamic structure of the coronal condensation from observations of the coronal lines come mainly from the superposition of a variety of densities and temperatures in a line of sight Therefore it is not possible to determine the physical state of the coronal condensation at each point along a line of sight without a reasonable assumption on its geometry

Aly et al. (1962), assuming axial symmetry for an enhance-

ment of the 1952 eclipse, determined the volume emissivity in the thirteen emission lines. They however failed to construct a single axially-symmetric model explaining the intensity distributions of these lines. Fisher (1972), relying on no geometrical assumption for a coronal enhancement of June 17, 1970, estimated mean temperatures in the lines of sight directly from the intensity ratios of the lines in the same ion class: I(FeX 6374)/I(FeXI 7892) and I(FeXIV 5303)/I(FeXIII 10747). The difference between these two mean temperatures was significant, and this must be a direct evidence for the superposition of different temperatures along a line of sight. Tsubaki (1975) also showed that the intensity ratios I(FeX 6374)/I(FeXI 7892) and I(FeXIV 5303)/I(FeXV 7059) give very different temperatures. Jefferies et al. (1972) formulated quite a general diagnostic procedure applicable to an optically thin gas. Giving up attempts to describe the geometrical model of a coronal formation, they represented its thermodynamic structure by means of the distribution function μ (Ne, T), where Ne is the electron density and T the temperature. In practice, however, incompleteness of observational data obliged them to take an approximate approach of determining the density-temperature relation and the temperature distribution function Φ(T), assuming some monotonic relation between Ne and T which is not always promised.

Our primary interest in studying the coronal condensation is to find not only its own physical structure but also its geometrical and thermodynamic relation to underlying or neigh-

boring phenomena in the active region. The monochromatic-image observations in various lines of different ionization potentials are most helpful for such a study (e.g. Dollfus (1971), Dunn (1971), Picat et al. (1973)). Boardman and Billings (1969) analyzed EUV spectroheliograms of a coronal condensation obtained by the Naval Research Laboratory on April 28, 1966. Although the absolute values of the temperature they obtained may be open to question because they used too high ionization temperatures compared with Jordan's (1969) calculation, they verified a type of condensation having a dense and hot core surrounded by a cooler halo.

At the total solar eclipse of June 30, 1973, the flash spectrograms of the chromosphere and corona were successfully obtained by the Kwasan and Hida Observatories Party. Since the dispersion of the spectrum is low enough, we can safely regard coronal lines of the flash spectrograms as the monochromatic images of the corona. On eclipse day the coronal condensation, associated with McMath Active Region 12397, was just onto the west limb In this paper we have analyzed the monochromatic images of the coronal condensation in FeXIV 5303, FeX 6374 and FeXI 7892 coronal lines and compared its thermal structure with other condensations in the light of the lifetime of the coronal active region

2. Observations

The Kwasan and Hida Observatories Party observed the total solar eclipse of June 30, 1973 at Atar, Mauritania of West Africa. The outline of our program and preliminary results have been described by Kanno (1973) and Kanno et al. (1974a). Only the essential aspects related to the flash spectrograms on which this investigation is based are summerized as follows.

Our slot-spectrograph is an improved version of the spectrograph used at the 1970 eclipse (Kanno et al., 1974b). The solar image of 41.8 mm in diameter was produced on the wide slot of the spectrograph by the coelostat system and the objective lens which has an aperture of 30 cm and a focal length of 450 cm. The light of the chromosphere and corona through the entrance slot was collimated by a lens (ϕ = 14 cm, f = 70 cm) and dispersed with the grating of 600 grooves mm^{-1} Then the spectra from 4600 to 6800 Å and from 7670 to 8130 Å were focused by a camera lens (ϕ = 14 cm, f = 70 cm) on Kodak Tri-X Aercon Film and 35 mm High Speed Infrared Film respectively with an average dispersion of 19.5 Å/mm. The motor-driven cameras, controlled by the programing device, performed continuous runs of exposures from 60 s before, till 50 s after second contact and also from 32 s before, till 60 s after third contact. The exposure times of the flash spectra ranged from 0.21 s to 1.96 s for the visual region and from 0.26 s to 8.0 s for the infrared region. The spectra obtained were of fine quality (see Kanno, 1973), some of which are shown in Figure 1 (a), (b). The absolute intensity scale was determined by the spectra of the partial Sun by fitting them to the existing

limb darkening data (Kanno et al., 1974b).

3. The Monochromatic Images of the Coronal Lines

The feature selected for study is the coronal condensation at the west limb of the Sun whose associated McMath No. 12397 active region was just onto the limb on eclipse day. This coronal condensation can be clearly noticed in the three coronal lines of 5303, 6374 and 7892 Å together with a conspicuous streak of the continuum on the flash spectrograms of the third contact (Figure 1 (a), (b)). Since the dispersion of the spectra is low enough, the line broadening due to thermal and nonthermal motions of the gas in the line of sight is completely negligible comparing with the spatial extent of the corona. Therefore we can safely regard the images of coronal lines on the flash spectrograms as the monochromatic images of the coronal structure (Kanno, 1975). Two frames of the flash spectrograms which are of the best quality near the third contact, were selected and studied by means of detailed photometry of the monochromatic images of the coronal condensation. These were exposed at $10^h\ 50^m\ 12.78^s$ UT (Frame No. III-13) and $10^h\ 50^m\ 12.0^s$ UT (Frame No. IRIII-8) in the visual and infrared regions, respectively, about 4 s before third contact (Figure 1 (a), (b)). The images of the coronal condensation in 5303, 6374 and 7892 Å were traced along the direction of the dispersion by the step of about 3000 km on the Sun with the microphotometer of the Department of Astronomy,

University of Kyoto. The slit size of the microphotometer was 25 μ wide and 100 μ long, which corresponded to 820 km and 3300 km on the Sun.

The resultant iso-surface-brightness maps (hereafter to be called ISBM) of the coronal condensation in the monochromatic light of the coronal lines are shown in Figure 2 (a), (b) and (c). In order to find the absolute intensity in units of erg cm^{-2} sec^{-1} $steradian^{-1}$ the values in the maps must be multiplied by the factors of 17.6, 4.33 and 16.1 for the 5303, 6374 and 7892 lines, respectively. On the original films of the flash spectrograms the image size along the dispersion is minified by adopting a grazing incidence for the grating. In Figure 2, however, the scale of length is corrected for the minification. The position of the Moon's limb on the ISBMs was determined by smoothly linking the points where the surface brightnesses increase most sharply. The three heights of 17000, 30000 and 50000 km above the Sun's limb are also shown. We shall examine the physical structure of the coronal condensation at these heights in detail in the following sections But some global aspects of the condensation can be directly deduced from ISBMs and summarized as follows

(1) This coronal condensation has, roughly speaking, a hemisphere-like structure as a whole with a radius of about 9×10^4 km.

(2) At a glance the ISBMs in three coronal lines seem to be nearly in an axially-symmetric structure. In order to examine this in more detail, the axis of symmetry of the ISBM in 5303 Å

is estimated as shown in Figure 2 (a), (b) and (c) by broken lines. It can be noticed in Figure 2 (b), (c) that the central line of the 5303 structure passes just through the centers of the 6374 and 7892 structures at the heights lower than 30000 km, but that the central line of the 5303 structure noticeably deviates from that of 6374 at the heights higher than 30000 km.

(3) The surface brightness in ISBMs shows maximums at the heights of 16000, 17000 and 19000 km for 5303, 6374 and 7892, respectively. Since the differences of these heights are within the errors in defining the position of the lunar limb on ISBMs, we may infer from ISBMs that this coronal condensation has a maximum surface brightness in three lines at the same height; about 17000 km. A closer examination of this height will be given below.

(4) While the positions of the maximum surface brightness in 6374 and 7892 lines coincide exactly with each other, the 5303 structure has two peaks of the surface brightness at both sides of the 6374 and 7892 peaks.

We have above inferred from ISBM that the surface brightness in the 6374 line reaches its maximum at the height of 17000 km of the position angle 258°. However, since the corona lower than about 9000 km was yet eclipsed by the Moon at the position angle 258° when the frame No. III-13 was exposed, and also since the atmospheric, instrumental, and photographic blurrings make ISBM near the lunar limb unreliable, we cannot decide from Figure

2 (b) whether there occurs any greater value of the surface brightness lower than 17000 km. In order to settle the question, we constructed the so-called eclipse curve of the 6374 line at the position angle 258°. The microphotometric tracings were made on all the spectrograms of the third contact. The integrated intensities of the 6374 line,

$$E(H) = \int_H^\infty I(h)\, dh \quad , \tag{1}$$

are shown as a function of height H in Figure 3, where the broken line represents the mean curve of the measured points, viz., the so-called eclipse curve of the 6374 line. It is naturally seen from Equation (1) that the negative gradient of the eclipse curve gives the surface brightness in the 6374 line at each height. The straight line in Figure 3 shows the gradient corresponding to the maximum surface brightness of 250 erg $cm^{-2} s^{-1}$ sterad^{-1} in the Figure 2 (b). It can be found that there appears no gradient larger than that of this straight line in the eclipse curve. In consequence we can safely conclude that this coronal condensation has the maximum surface brightness in the 6374 line at the height of 17000 km above the solar limb.

4. Basic Equations of the Coronal Line Emission

The surface brightness I_λ given in Figure 2 is the integral of the emmisivity $\varepsilon_\lambda(z)$ over the line of sight, i.e.,

$$I_\lambda = \int_0^\infty \varepsilon_\lambda(z)\, dz \quad , \qquad (2)$$

in which the volume emissivity $\varepsilon_\lambda(z)$ may be expressed by

$$\varepsilon_\lambda(z) = \frac{h\nu}{4\pi} N_2 A_{21} = \frac{hc}{4\pi} \frac{A_{21}}{\lambda} \frac{N_2}{N_{ion}} \frac{N_{ion}}{N_{Fe}} \frac{N_{Fe}}{N_H} \frac{N_H}{N_e} N_e \, , \qquad (3)$$

where A_{21} is the spontaneous transition probability, N_2 the upper level population of the relevant transition, N_{ion} the concentration of the ion in question, N_{Fe}/N_H the abundance of iron relative to hydrogen, and Ne the electron density.

The theoretical calculations for the excitation of coronal lines of iron were recently performed by several authors (Zirker, 1970, Blaha, 1971, De Boer et al., 1972, and Noëns and Rozelot, 1974). According to their calculations the excitation of the lines in question are insensitive to temperature but very sensitive to electron density Fortunately, however, the ratios $(N_{XIV\cdot2}/N_{XIV})/(N_{X\cdot2}/N_X)$ and $(N_{XI\cdot2}/N_{XI})/(N_{X\cdot2}/N_X)$ are found to remain practically constant over a range of $10^8 < Ne < 10^{10}$, where $N_{X\cdot2}/N_X$, N_{XI2}/N_{XI}, and N_{XIV2}/N_{XIV} are the excitation ratios for the upper levels of 6374, 7892 and 5303 lines. According to Zirker's calculation, $(N_{XIV2}/N_{XIV})/(N_{X2}/N_X)$ varies from 1.97 to 2.3 and $(N_{XI2}/N_{XI})/(N_{X2}/N_X)$ from 2.6 to 1.6 respectively over a range of $10^8 < Ne < 10^{10}$, so that we have without any serious error

$$\frac{\left(\frac{N_{XIV\cdot2}}{N_{XIV}}\right)}{\left(\frac{N_{X2}}{N_X}\right)} = 2.1 \qquad \text{and} \qquad \frac{\left(\frac{N_{XI2}}{N_{XI}}\right)}{\left(\frac{N_{X2}}{N_X}\right)} = 2.5 \, . \qquad (4)$$

From Equations (3) and (4) we get

$$\log(N_{XIV}/N_X) = \log(\varepsilon_{5303}/\varepsilon_{6374}) - 0.342, \quad (5)$$

$$\log(N_{XI}/N_X) = \log(\varepsilon_{7892}/\varepsilon_{6374}), \quad (6)$$

and

$$\log(N_{XIV}/N_{XI}) = \log(\varepsilon_{5303}/\varepsilon_{7892}) - 0.342, \quad (7)$$

where we adopted $A_{21}(5303) = 60$, $A_{21}(6374) = 69$, and $A_{21}(7892) = 34$.

According to the theoretical calculations of the ionization equilibrium for coronal ions, the degree of ionization depends upon the electron temperature alone. Using Jordan's (1969) extensive calculation for ionization equilibrium we can obtain the temperature structure of the coronal condensation from Equations (5), (6), and (7) if the volume emmisivities ε_{5303}, ε_{6374}, and ε_{7892} are given from the observation.

In the next place, adopting the abundance of iron $N_{Fe}/N_H = 4.68 \times 10^{-5}$ (Withbroe, 1971), Equation (3) may be written as

$$\log N_e A_{6374}(N_{X2}/N_X) = \log \varepsilon_{6374} - \log(N_X/N_{Fe}) + 17.03, \quad (8)$$

$$\log N_e A_{5303}(N_{XIV2}/N_{XIV}) = \log \varepsilon_{5303} - \log(N_{XIV}/N_{Fe}) + 16.95, \quad (9)$$

and

$$\log N_e A_{7892}(N_{XII}/N_{XI}) = \log \varepsilon_{7892} - \log(N_{XI}/N_{Fe}) + 17.12 , \quad (10)$$

where we assumed $N_H/N_e = 0.8$. Since the values of N_{ion}/N_{Fe} can be found from Jordan (1969) for the temperature determined above, we can obtain the electron density structure from the observed value of ε_λ by means of Equations (8) through (10).

5 Ne and T Structure of the Condensation

In this section we shall examine the surface brightness distributions of the three coronal lines of Figure 2 at various heights and solve the Ne and T structure of this coronal condensation by using the procedure developed in Section 4.

A. AT THE HEIGHT OF 17000 KM

The surface brightnesses at the height of 17000 km above the solar limb are plotted against the position angle for the 5303, 6374 and 7892 lines in Figure 4 (a). These surface brightness distributions of all the three lines show fairly good symmetry with respect to the position angle 258° which is centered in the abscissa of Figure 4. Thus, assuming that this condensation has an axially-symmetric structure at the height of 17000 km, we can find the volume emissivity as a function of distance from the axis of symmetry Aller (1956) gives a good illustration of this method applied to planetary nebulae. Aly et al. (1962) applied this method of analysis to the study of the coronal condensation

of the 1952 eclipse.

We assumed that the condensation is composed of 20 concentric shells each having the same thickness Δx and a constant value of emissivity ε_j . According to this model, Equation (2) is replaced by a set of simultaneous equations

$$I_i = 2\Delta x \sum_{j \geq i}^{20} a_{ij}\, \varepsilon_j \quad (1 \leq i \leq 20) \ , \qquad (11)$$

where

$$a_{ij} = \sqrt{(j+1)^2 - i^2} - \sqrt{j^2 - i^2} \quad (j \geq i) . \qquad (12)$$

Then the emmisivity of each shell is expressed by the matrix equation

$$2\Delta x(\varepsilon_j) = (I_i)\,(\overline{a_{ij}}) \quad (1 \leq i, j \leq 20) , \qquad (13)$$

where $(\overline{a_{ij}})$ is the inverse of the matrix (a_{ij}).

Although the left and right halves of the surface brightness distribution in Figure 4 (a) are slightly different from each other, a preliminary analysis of each half confirmed that these differences in the surface brightness distributions bring about little change in the essential physical characteristics of the condensation. Therefore we analyzed the left half of the surface brightness distribution in Figure 4 (a) deviding the region from the position angle 258° to 250° into 20 divisions. In order to obtain the surface brightness of the coronal condensation itself,

the surface brightness of the nearby normal region was subtracted from those in Figure 4.

The emissivity distributions obtained by (13) are shown in Figure 5 in units of 10^{-8} erg cm^{-3} s^{-1} $sterad^{-1}$, where vertical bars show the range of errors due to the ambiguity in smoothing the I(x) profiles in Figure 4 (a). Only the upper limit of the emissivity could be determined at the center of the 5303 structure. It is noticed that the 6374 emissivity has a maximum at the center of the condensation and abruptly decreases outward. On the contrary the 5303 line has little emissivity at the center and shows the maximum emissivity at the intermediate region of the symmetric structure. The emissivity distribution of the 7892 line is rather similar to that of the 6374 line as a whole, but shows a much slower decrease from the center to the outer boundary of the condensation.

Substituting these emissivities into Equations (5) to (7), we can obtain the ion population ratios and the temperature by using the calculations of Jordan (1969). In this way the resultant temperature distributions in the condensation are shown in Figure 6 (a). Since the temperature obtained from the 6374/7892 pair is most seriously affected by the probable errors of the emissivity in Figure 5, the vertical bars showing the ambiguity of the temperature are given only for this pair in Figure 6 (a). The three temperature distributions obtained from the different line pairs are as a whole in a general agreement; these all show about 10^6 K at the central region, about 2×10^6 K around the intermediate region and fall off to about 1.5×10^6 K near the

outer boundary.

Next, we determined the electron density distributions according to Equations (8) to (10), where we adopted the mean temperature distribution shown by the solid line in Figure 6 (a). The resultant electron density distributions are shown in Figure 6 (b), where the vertical bars show the range of ambiguity corresponding to the probable errors in the emissivity and temperature obtained above. Although a fairly large ambiguity is seen around the region about 24000 km apart from the center (which is mainly due to the large temperature ambiguity at the sharply increasing temperature region), the three electron density distributions obtained from the different lines are generally in a good agreement with each other, especially between 5303 and 6374 lines; these show about 6×10^9 cm^{-3} at the center, about 3.5×10^9 cm^{-3} at the intermediate region and fall off to about 6.5×10^8 cm^{-3} at the outer boundary of the condensation.

In conclusion we could successfully determine the mean Ne and T distributions of the axially-symmetric structure which are consistent with the observed surface brightness distributions of the three coronal lines 5303, 6374 and 7892 Å except a relatively large ambiguity in the sharply increasing temperature region. It is noticed that a cool and dense core region ($T = 10^6$ K and $Ne = 6 \times 10^9$ cm^{-3}) is a very striking feature in this coronal condensatio

B. AT THE HEIGHT OF 25000 KM

The same procedure as used in Subsection A was applied to the surface brightness distribution at the height of 25000 km. The results are generally similar to those for the height of 17000 km, and the axial symmetry seems to be a reasonable assumption also at this height. Only the final result of the mean Ne and T structure of this height is given in Figure 8. A cool and dense core is striking also at the height of 25000 km.

C. AT THE HEIGHT OF 30000 KM

The surface brightness distribution at the height of 30000 km also shows nearly perfect symmetry (Figure 4 (b)), whose left half was selected to be analyzed by the same way. The resultant temperature distributions are given in Figure 7 (a). Two temperature distributions from the 5303/6374 and 5303/7892 pairs are in a good agreement over the whole region, but the one from the 7892/6374 pair shows fairly large difference from the other two. This implies that the errors of the emissivity obtained with the assumption of a single axially-symmetric structure may be rather significant at this height. Since the temperature determined from the 7892/6374 pair is much more seriously affected by the errors of the emissivity than the other two pairs, we defined a mean temperature distribution only from the latter two. The electron density distribution was determined from the mean temperature and shown in Figure 7 (b) A cool and dense core can still be recognized at this height, but the temperature gradient around the central region becomes much less steep than at the lower height.

D. AT THE HEIGHT OF 50000 KM

In Figure 4 (c) it can be noticed that the surface brightness distribution of the 5303 line shows no central dip, and that the position of the central peak of 6374 slightly deviates from the other two. This deviation has already been found in the ISBMs in Section 3 and may indicate that a single axially-symmetric model is inadequate to explain the surface brightness distributions of all these lines at this height. But the surface brightness distributions in the 5303 and 7892 lines, both still showing good symmetry, should be used to determine an axially-symmetric structure of Ne and T which may not be so far from the real physical condition at this height. The resultant temperature and density distributions are shown in Figure 8. It should be noticed that there exists no cool core and that the central region has higher temperatures and higher densities at this height. An examination of the height of 60000 km yielded a similar result, so that the cool and dense core seems to exist only below the height of about 40000 km.

6. Monochromatic Image in $H\alpha$ Line

It would be very interesting to study the interaction between the corona and the chromospheric or prominence matter in the active region. In Figure 1 (a) some chromospheric or prominence-like formations can be seen in $H\alpha$ line at the same region as the coronal condensation. Thus we also made the ISBM of the mono-

chromatic image in H_α line by the same procedure as in the coronal lines and superposed it on the ISBM of the 6374 coronal line as shown in Figure 9.

One is much impressed to find that the columnar H_α structure protruding from the active chromosphere is in a good coincidence with the region of the maximum surface brightness in the 6374 line or the cool and dense core of the coronal condensation. At Kwasan Observatory Kubota (1973) observed that small active H_α structures, as shown in Figure 1 (d), repeatedly appeared and diminished at the very region studied here. We can safely regard these as the same type of structures as that of H_α structure in Figure 9.

Such columnar H_α structures can be frequently seen to protrude from the plage region almost every time when an active region comes onto the limb. They often appear in group and some of them have a close interaction with coronal rains (Kawaguchi, 1970). Lüst and Zirin (1960) found that by proper choice of the compression rate the coronal matter of $T = 1 \sim 2 \times 10^6$ K and $Ne = 10^9 \sim 10^{10}$ cm^{-3} may well form an active prominence in a reasonable time scale.

At the present stage, however, we do not know whether these H_α structures in question originate from the underlying plage region or are condensed out of the corona. We can only emphasize the striking spatial coincidence between the cool and dense core of the coronal condensation and the columnar H_α structure protruding from the plage region as seen in Figure 9.

7. Discussion

In the monochromatic images of the three coronal lines, 5303, 6374 and 7892 Å, the coronal condensation studied here seems to have a hemisphere-like structure with the height of about 9×10^4 km. However, we should always keep it in mind that this coronal condensation corresponds to the innermost part of the coronal enhancement seen in the white light photograph of Figure 1 (c).

In the preceeding sections the assumption of the axial symmetry was successfully applied to the study of the density and temperature structure of the condensation, especially at the lower heights. The final results are summarized in Figure 8. Note that T and Ne obtained for the outer boundary of the condensation are both in good agreement with the current estimates of electron temperature and electron density for the normal corona.

Generally speaking, the temperature of this coronal condensation is not high and there is no evidence for the presence of the material with higher temperatures than 2.3×10^6 K even if the possible errors of analysis are taken into account. On the contrary, this coronal condensation is strongly characterized by the existence of a cool and dense core with the minimum temperature of about 10^6 K and the maximum density of about 6×10^9 cm^{-3}. Such a cool and dense structure in the corona has never been quantitatively verified before this study, though Dollfus (1971) gave an example of a similar cool conic structure of the corona in his study of the monochromatic images of the 5303 and 6374 lines.

In the central region of this coronal condensation the mean temperature gradient along the horizontal direction reaches a maximum value of 10^6 K/4.5×10^4 km = 2.2×10^{-4} K/cm at the height of 17000 km. Such a temperature gradient is very large in the corona and implies the presence of the substantial magnetic field suppressing thermal conduction.

The gas pressure at the height of 17000 km amounts to $2kNeT = 1.7$ dyn cm^{-2} for the central region and about 1.9 dyn cm^{-2} for the intermediate region, both of which are about ten times as large as that in the quiet region of the lower corona. On the other hand the magnetic field strength might be about 8.5 Gauss, if the equipartition between kinetic and magnetic energy is assumed. However, this value of the magnetic field at the height of 17000 km might be rather small compared with the current estimates of the coronal magnetic fields above the active region according to Newkirk's summary (1967). In any case this coronal condensation should be substantially controlled by the magnetic field.

In examining various types of coronal condensation, we should always pay attention to their evolution. Neupert (1967) noticed from the EUV line data of OSO-I that the observed highest stages of ionization (FeXVI) are most prominent early in the lifetime of the active region and that FeXIV and lower stages of ionization become predominant as activity subsides. Figure 10 shows the daily variations of the 9.1 cm radio intensity, the plage area and the number of flares, quoted from Solar Geophysical Data, which demonstrate the evolution of McMath Region 12397 above which

our coronal condensation was situated; this active region passed its most active phase between June 22 and 26 and was in the declining phase of activity on eclipse day (June 30). Therefore we consider that the coronal condensation studied here, which is characterized by a high electron density and not so high temperature, represents a type of condensation in the post maximum phase of activity. This is consistent with Neupert's (1967) conclusion.

Up to this time, emission line analyses of coronal enhancements have been presented by various authors. The coronal condensations of February 4, 1962 (Zirin, 1970) and April 28, 1966 (Boardman and Billings 1969) may represent one of the hottest types. The former was associated with a very active E type spot group, and the active region of the latter was fairly young. On the other hand the coronal condensations of May 30, 1965 (Jefferies et al., 1972 and Magnant-Crifo, 1974) and November 11, 1966 (Jefferies et al., 1972), both of which are relatively cool, were associated with the active regions in the declining phase of activity. These evidences also confirm Neupert's conclusion.

8. Conclusion

The coronal condensation observed at the June 30, 1973 eclipse has been studied in detail from the monochromatic images of the 5303, 6374, and 7892 lines in the flash spectrograms. Main results are summarized as follows.

(1) This coronal condensation has a hemisphere-like struc-

ture as a whole with a radius of about 9×10^4 km in the monochromatic images of the coronal lines and corresponds to the innermost part of the much larger coronal enhancement in the white light photograph.

(2) This coronal condensation has a maximum surface brightnesses in the coronal lines at the height of 17000 km above the solar limb.

(3) The electron density in the central region is about ten times as high as that of the normal corona at each height. But the temperature of the coronal condensation is not so high and there is no evidence for the presence of the material of higher temperature than 2.3×10^6 K.

(4) At the lower height (below about 40000 km) this coronal condensation has a cool and dense core (10^6 K, 6×10^9 cm^{-3} at 17000 km), and the small active prominenc protruding from the plage region is situated at just the same region.

(5) McMath Region 12397, above which this coronal condensation was situated, was in the declining phase of activity on eclipse day. Therefore the fairly high electron density and not so high temperature of this condensation represent a characteristic of a coronal active region in the post maximum phase of activity This is consistent with Neupert's (1967) conclusion on the evolution of the coronal active region.

Finally this investigation shows that monochromatic-image observations in various lines of different ionization potentials are most helpful for studying the coronal active region, not only morphologically, but also quantitatively, if a reasonable assump-

tion of geometry is made. Further investigations of this type are necessary for studying the active region in every evolutional stage.

Acknowledgements

The Kwasan and Hida Observatories Party (M. Kanno, T. Tsubaki, and the author) would like to express their gratitude to the Japanese Ministry of Education which allowed the grants for the expedition to République Islamique de Mauritanie of West Africa, and to the Eclipse Committee of the Science Council of Japan which gave cordial support to the eclipse expedition. The author wishes to thank Prof. S. Miyamoto, Prof. I. Kawaguchi and Drs. A. Hattori and M. Kanno for their constant encouragements and invaluable advice. The author is particularlly indebted to Dr. Kanno who made helpful suggestions throughout this work and read the manuscript.

References

Aller, L.H.: 1956, Gaseous Nebulae, John Wiley & Sons, New York, p. 256.

Aly, M.K., Evans, J.W., and Orrall, F.Q.: 1962, Astrophys. J. 136, 956.

Blaha, M.: 1971, Solar Phys. 17, 99.

Boardman, W.J and Billings, D.: 1969, Astrophys. J 156, 731.

De Boer, K.S., Olthof, H., and Pottasch, S.R.: 1972, Astron.

Astrophys. 16, 417.

Dollfus, A.: 1971, in C.J. Macris (ed.), Physics of Solar Corona, D. Reidel Publishing Co., Dordrecht, p. 97.

Dunn, R.B.: 1971, in C.J. Macris (ed.), Physics of Solar Corona, D. Reidel Publishing Co., Dordrecht, p. 114.

Fisher, R.R.: 1972, Solar Phys. 24, 385.

Jefferies, J.T., Orrall, F.Q., and Zirker, J.B.: 1972, Solar Phys. 22, 307.

Jordan, C.: 1969, Monthly Notices Roy Astron. Soc. 142, 501.

Kanno, M.: 1973, Sky Telesc. 46, 220.

Kanno, M.: 1975, to be submitted to Solar Phys.

Kanno, M., Tsubaki, T., and Kurokawa, H.: 1974a, Solar Eclipse 1973 Bulletin No. 5, N.S.F., Washington, p. 18.

Kanno, M., Tsubaki, T., and Kurokawa, H.: 1974b, Memoirs of the Faculty of Science, Kyoto Univ. 34, 281.

Kawaguchi, I.: 1970, Publ. Astr. Soc Japan 22, 405.

Kubota, J : 1973, private communication.

Lüst, R. and Zirin, H.: 1960, Z. Astrophys. 49, 8.

Magnant-Crifo, F.: 1974, Solar Phys. 39, 141.

Neupert, W.M.: 1967, Solar Phys. 2, 294.

Newkirk, G.: 1967, Ann. Rev Astron. Astrophys. 5, 213.

Noëns, J.C. and Rozelot, J.P.: 1974, Astron. Astrophys. 5, 213.

Picat, J.P , Fort, B., Dantel, M., and Leroy, J.L.: 1973, Astron. Astrophys. 24, 259.

Tsubaki, T.: to be published.

Withbroe, G.L.: 1971, in K.B. Gebbie (ed.), The Menzel Symposium

on Solar Physics, Atomic Spectra, and Gaseous Nebulae, NBS Special Publ. 353, p. 127.

Zirin, H.: 1970, Solar Phys. 11, 497.

Zirker, J.B.: 1970, Solar Phys. 11, 68.

Figure Captions

Fig. 1. (a) The parts of the flash spectrogram (Frame No. III-13) on which 5303, 6374 and H_α lines were measured. (b) The flash spectrogram (Frame No. IRIII-8) on which 7892 line was measured. These were exposed at about 4 s before third contact. (c) The white light photograph of the coronal enhancement whose innermost part was studied in this investigation. This was taken at $10^h\ 49^m\ 17^s$ UT. C indicates the coronal condensation and P a small prominence. (d) The H_α image of McMath No. 12397 active region obtained at Kwasan Observatory at $06^h\ 04^m$ UT on eclipse day (see Section 6).

Fig. 2. The iso-surface-brightness maps of the coronal condensation. (a) FeXIV 5303, (b) FeX 6374, (c) FeXI 7892. The position of the Moon's limb and the three heights of 17000, 30000, and 50000 km above the Sun's limb are shown.

Fig. 3. The eclipse curve of the 6374 line at the position angle 258°. The broken line represents the mean curve of measured points and the straight line shows the gradient corresponding to the maximum surface brightness in Figure 2 (b).

Fig. 4. The surface brightness distribution at three heights plotted against the position angle which is expressed by the difference from 258°. Circles for 5303, dots for 6374, and crosses for 7892.

Fig. 5. Emissivity distributions at the height of 17000 km. The abscissa is the distance from the axis of symmetry. Circles for 5303, dots for 6374, and crosses for 7892. Vertical bars show the range of errors. Only the upper limit could be determined at the center of the 5303 structure.

Fig. 6. The temperature and electron density distributions at the height of 17000 km. The abscissa is the distance from the axis of symmetry. Vertical bars show the range of the probable errors. (a) The temperature distribution. Circles show the temperatures obtained from the 5303 and 7892 pair, dots from the 5303 and 6374 pair, and crosses from the 6374 and 7892 pair respectively. The solid curve shows the mean temperature distribution. (b) The density distributions. Circles show the densities obtained from 5303, dots from 6374, and crosses from 7892.

Fig. 7. Same as Fig. 6, but for the height of 30000 km.

Fig. 8. The mean Ne and T distributions of the coronal condensation at four different heights. The abscissa is the distance from the axis of symmetry

Fig 9. The ISBM of the monochromatic image in H_{α} line (dotted curves) superposed on the ISBM in 6374 (solid curves).

Fig. 10. The evolution of McMath Region 12397. The upper figure

shows the daily variations of the plage area (open circles, in unit of 10^{-6} hemisphere) and the 9.1 cm radio intensity (filled circles, in unit of $10^{-22} Wm^{-2} Hz^{-1}$). The lower figure shows the flare activities in McMath Region 12397, where circles show identified flares and crosses unidentified flares. (Quoted from Solar Geophysical Data.)

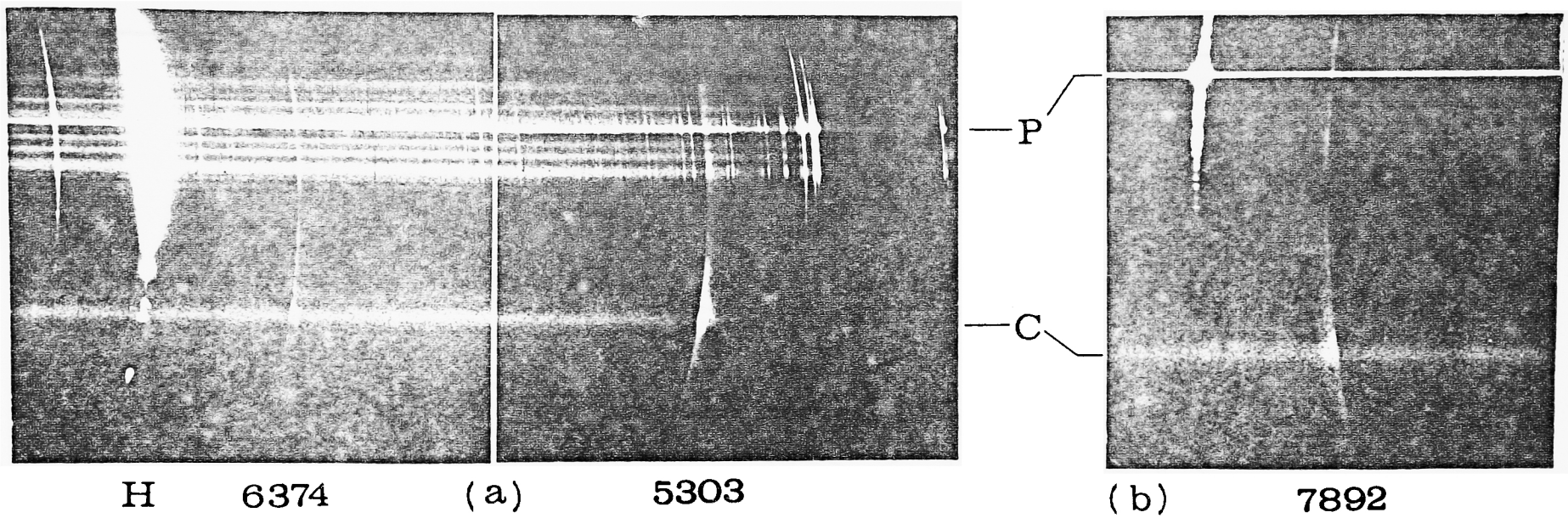
P
C
H 6374 (a) 5303
(b) 7892
(c)
C
P
(d)

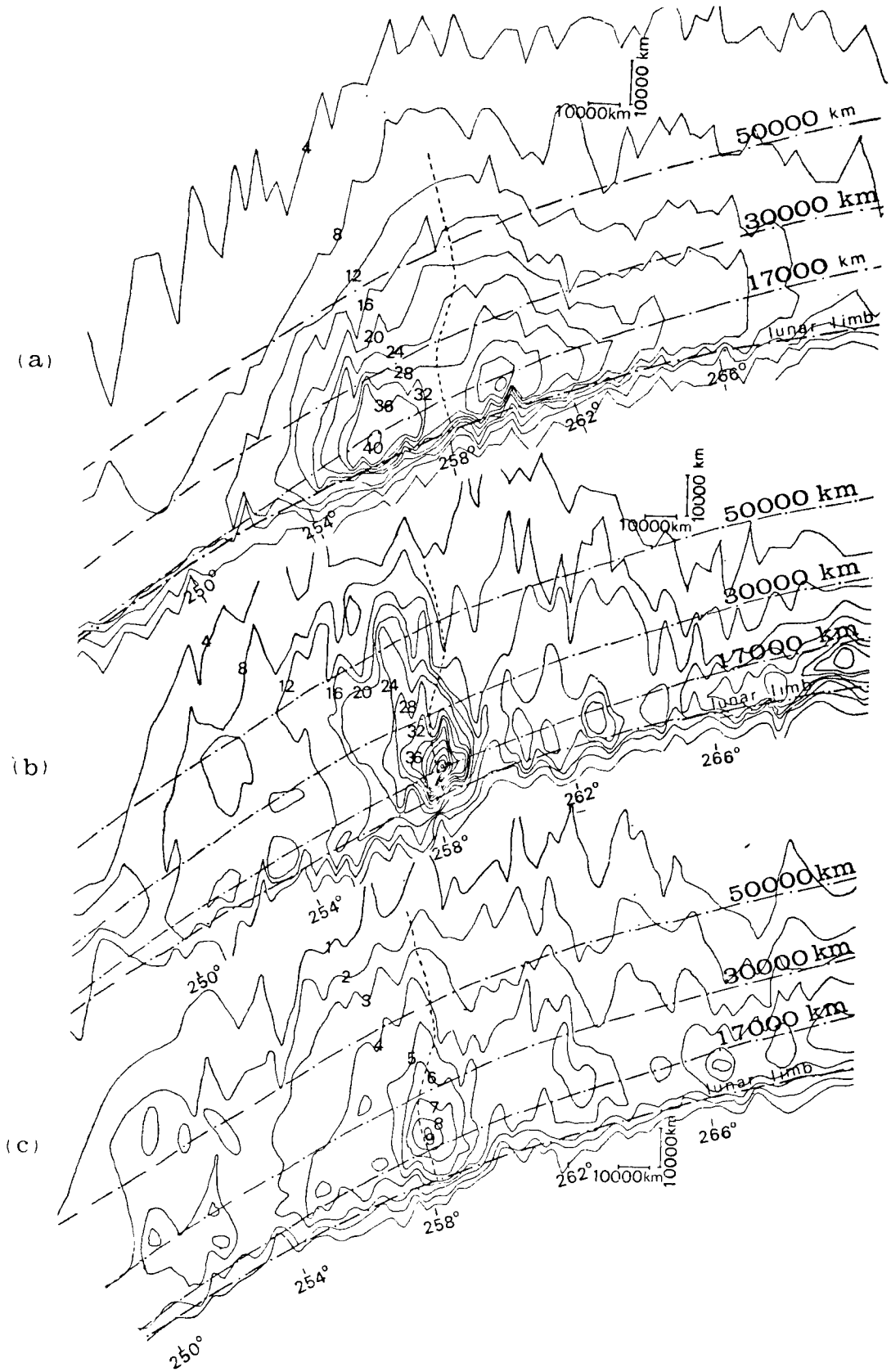
(a)
(b)
(c)
10000km
10000 km
50000 km
30000 km
17000 km
Lunar Limb
4
8
12
16
20
24
28
32
36
40
250°
254°
258°
262°
266°
2
3
5
6
7
9

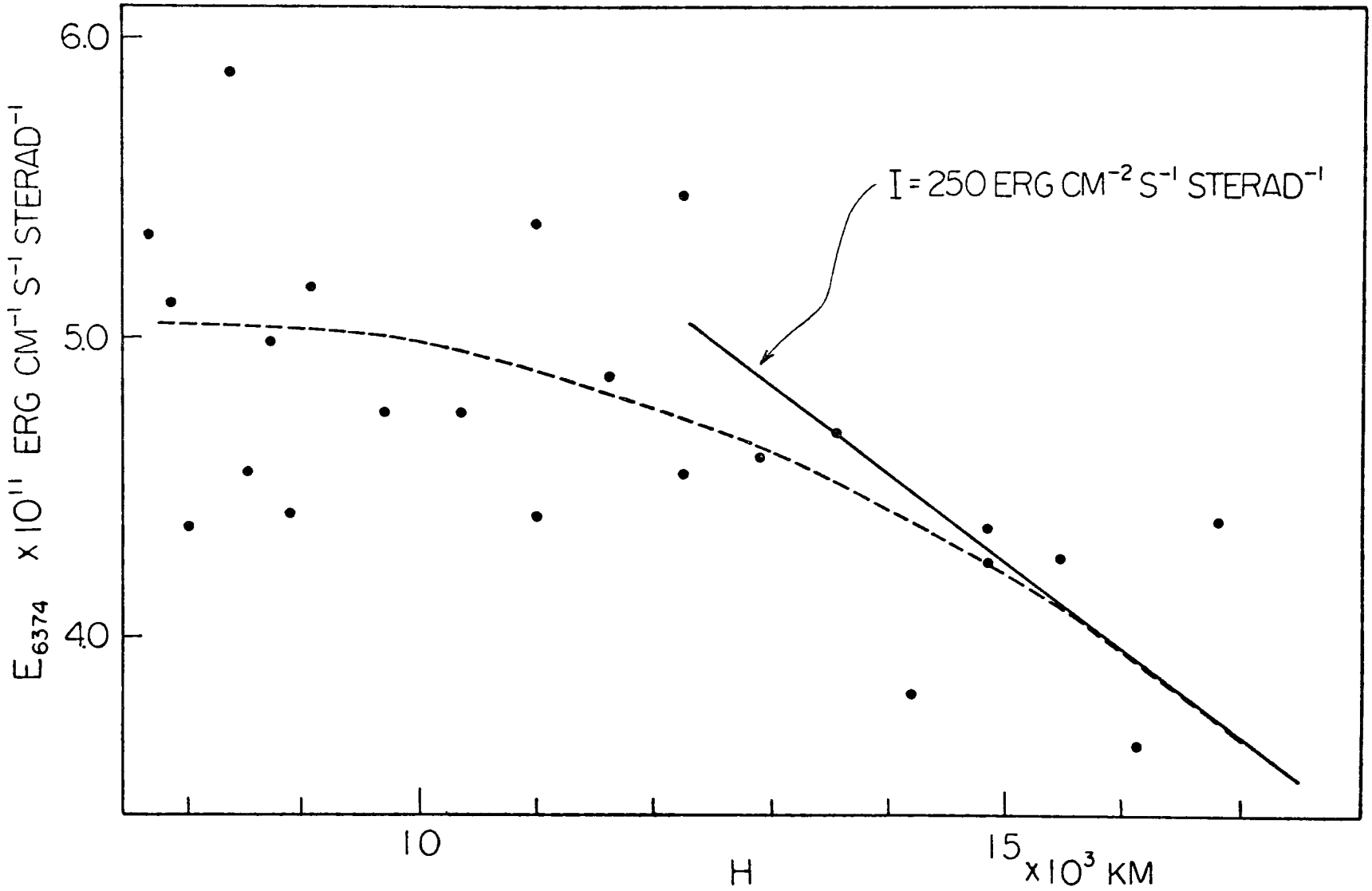
6.0
5.0
4.0
E_{6374} x 10^{11} ERG CM^{-1} S^{-1} STERAD^{-1}
I = 250 ERG CM^{-2} S^{-1} STERAD^{-1}
10
15
H
x 10^3 KM

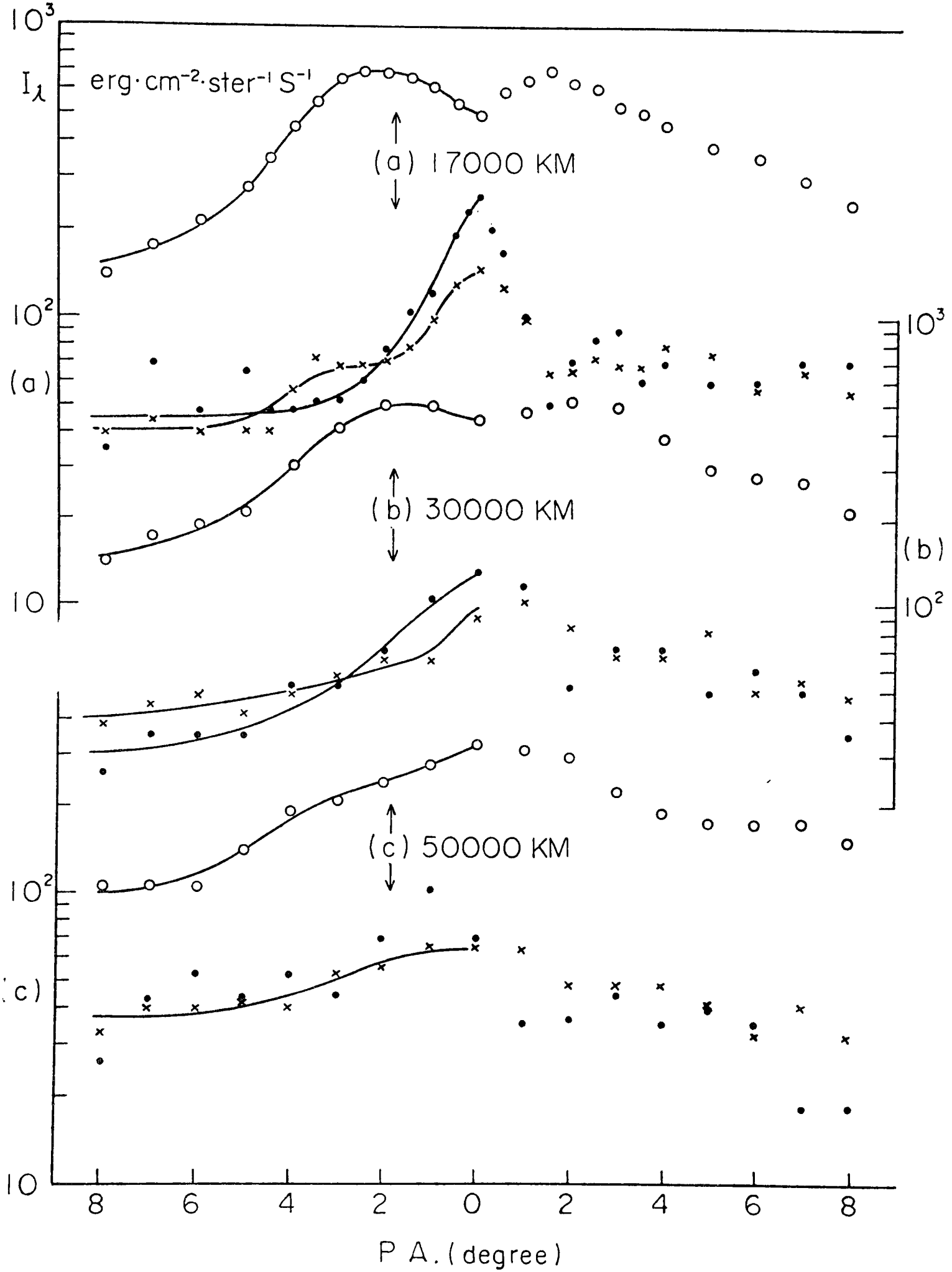
10^3
I_λ
erg·cm^{-2}·ster^{-1} S^{-1}
(a) 17000 KM
10^2
(a)
(b) 30000 KM
10
(b)
10^3
10^2
(c) 50000 KM
10^2
(c)
10
8
6
4
2
0
2
4
6
8
P A. (degree)

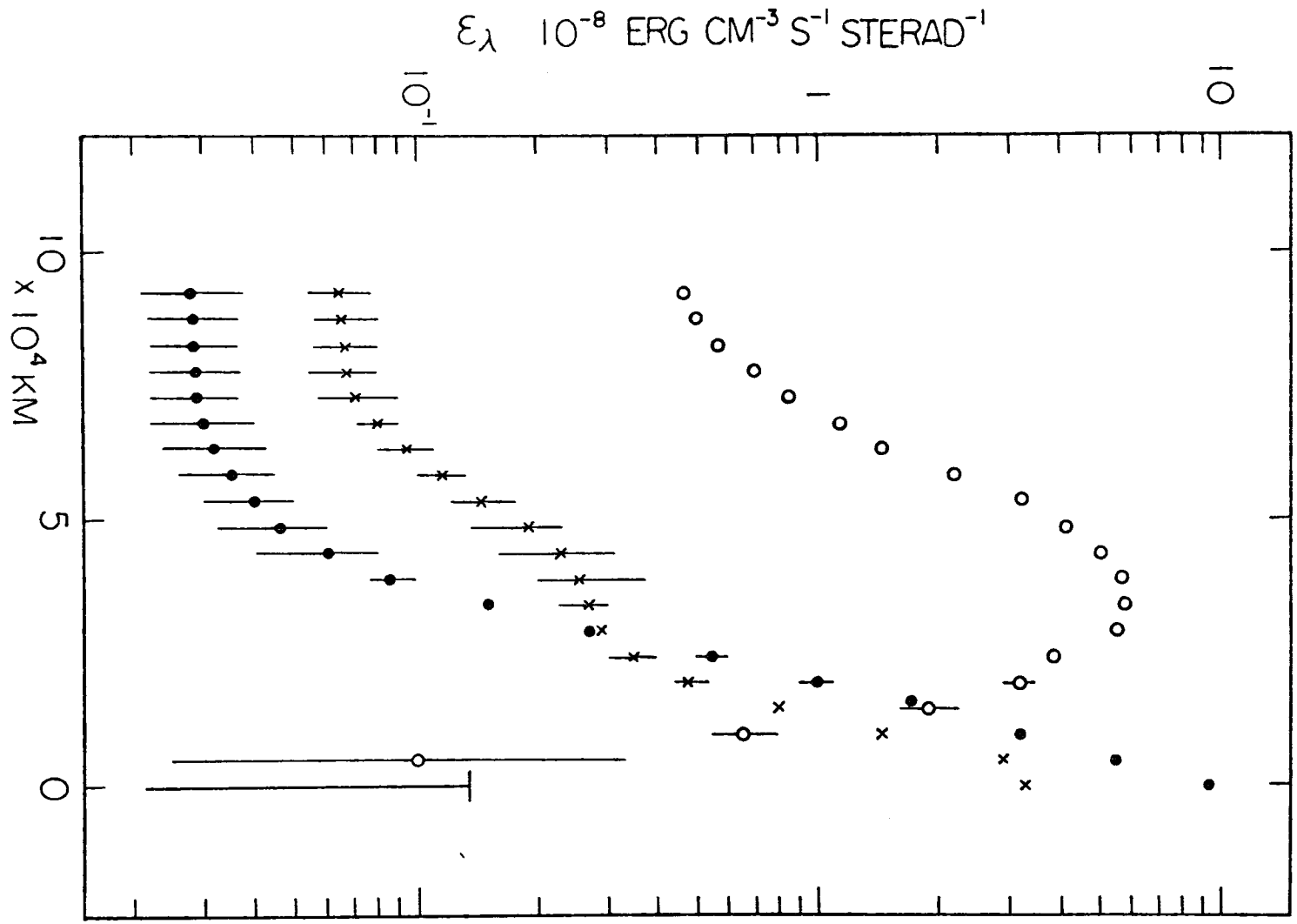
ε_λ 10^{-8} ERG CM^{-3} S^{-1} STERAD^{-1}
$\overline{10}_{-1}$
—
$\overline{10}$
10
5
0
$\times 10^4$ KM

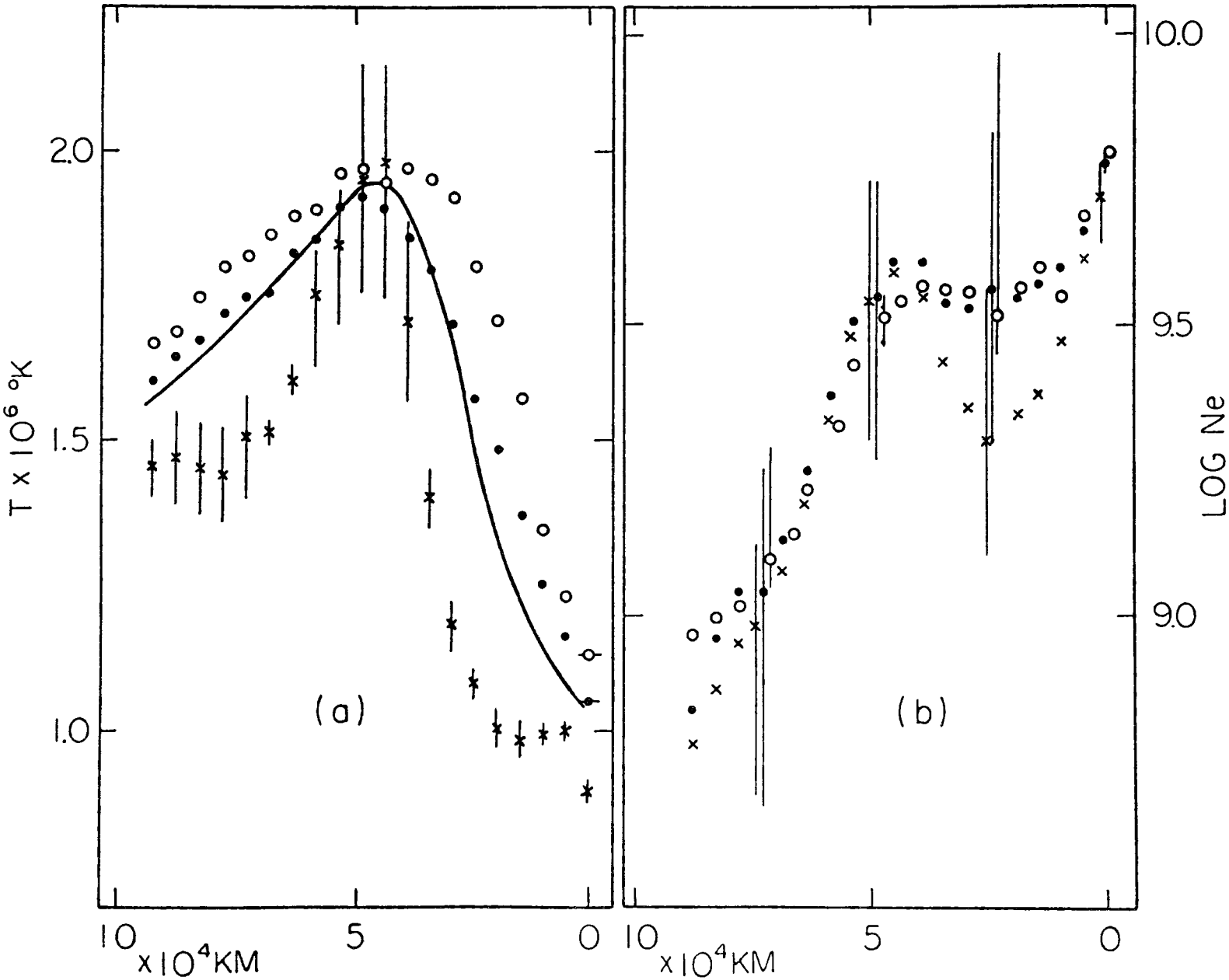
2.0
1.5
1.0
T x 10^6 °K
(a)
10
5
0
x10^4KM
10.0
9.5
9.0
LOG Ne
(b)
10
5
0
x10^4KM

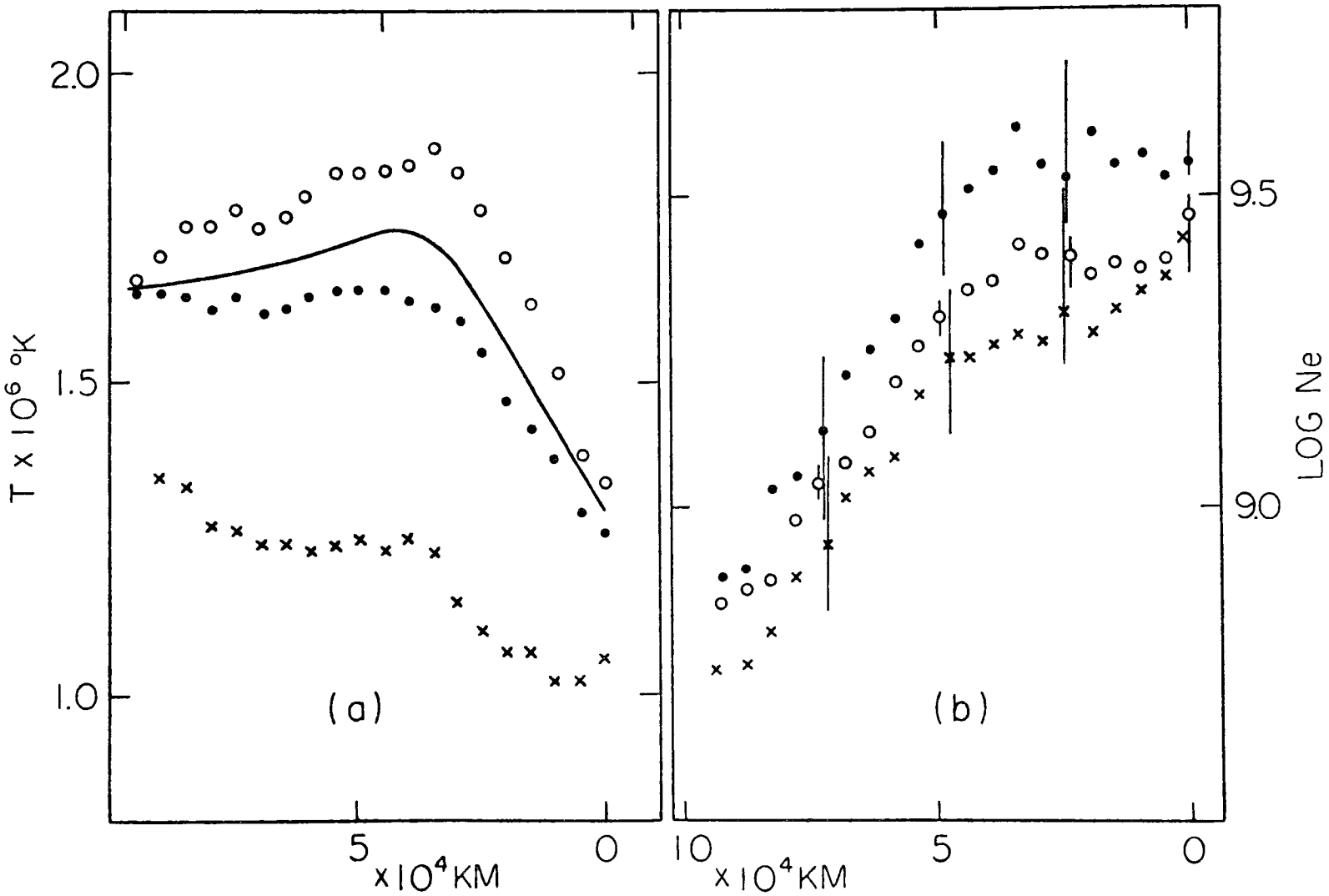
2.0
1.5
1.0
T x 10^6 °K
(a)
5
0
x 10^4 KM
10
5
0
x 10^4 KM
(b)
9.5
9.0
LOG Ne

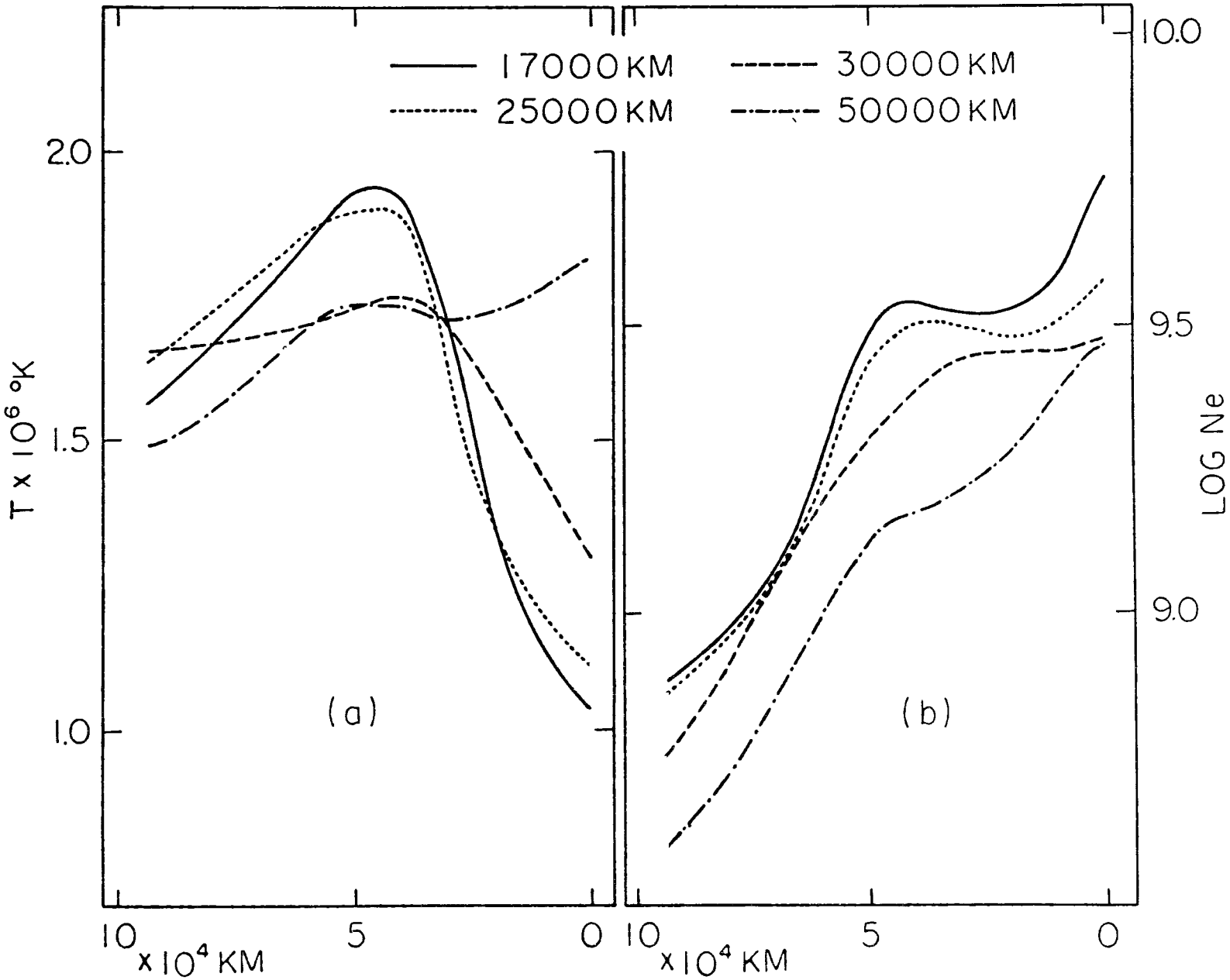
17000 KM
25000 KM
30000 KM
50000 KM
2.0
1.5
1.0
T x 10^6 °K
10.0
9.5
9.0
LOG Ne
(a)
(b)
10
5
0
x 10^4 KM

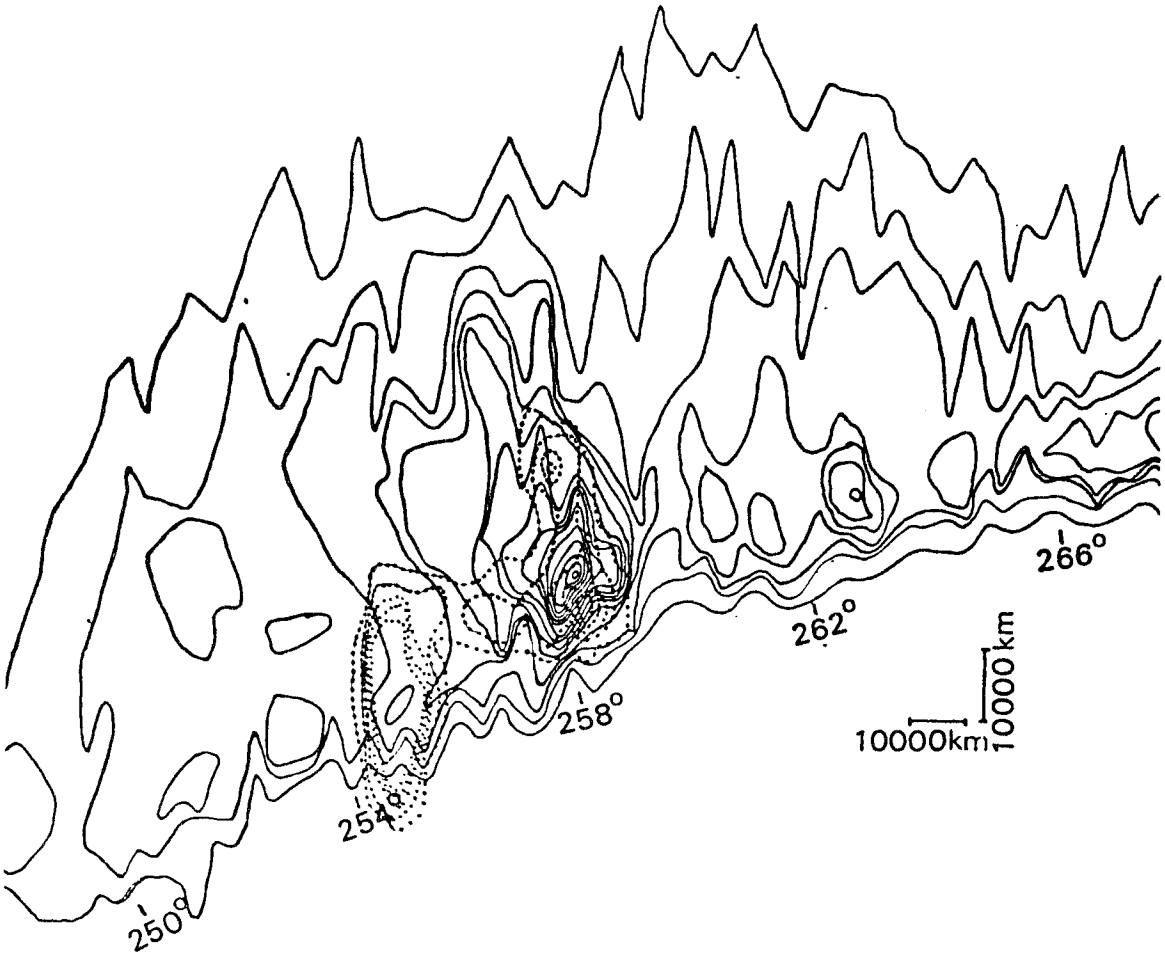
250°
254°
258°
262°
266°
10000km
10000km

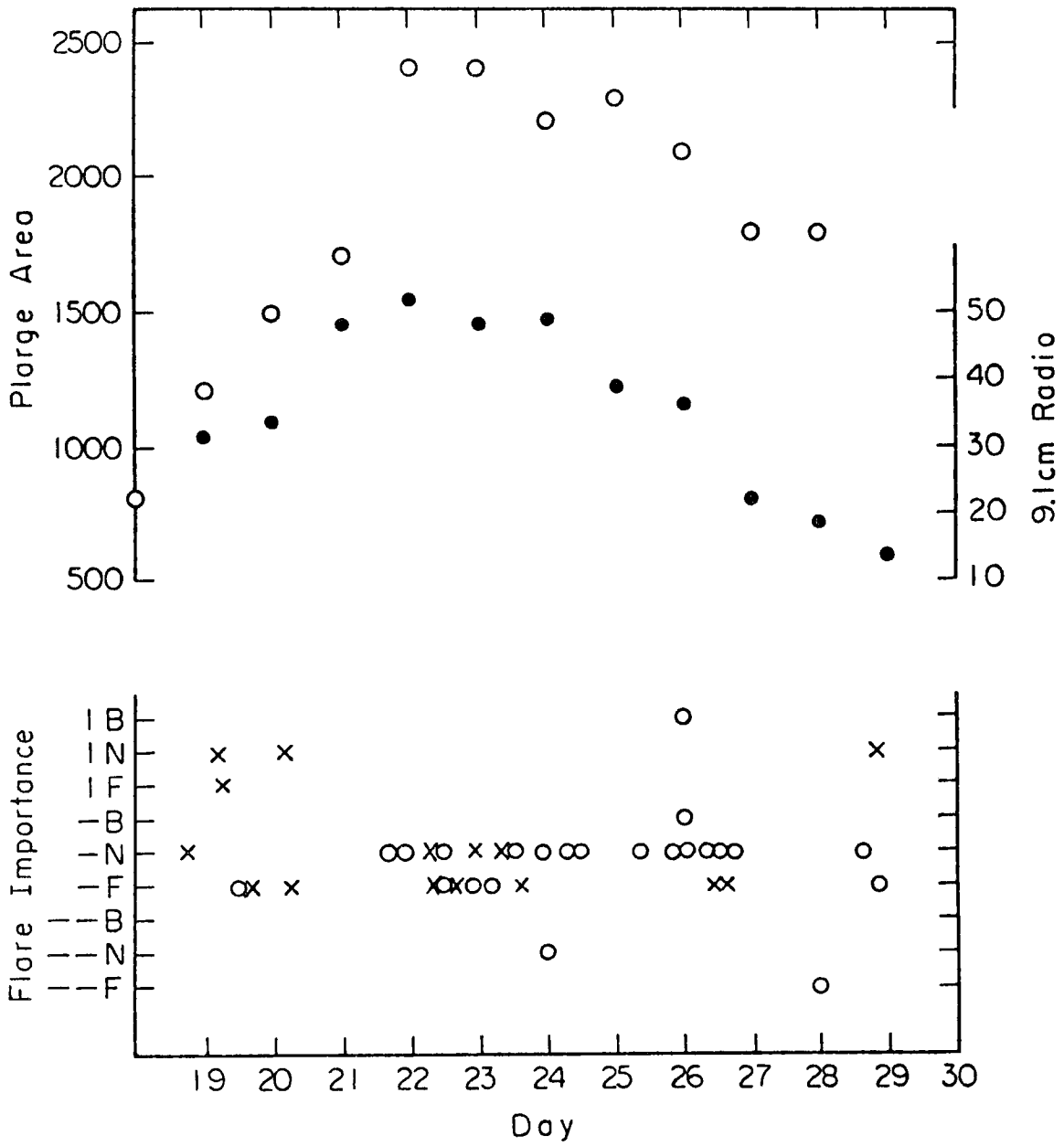
2500
2000
1500
1000
500
Plarge Area
50
40
30
20
10
9.1cm Radio
1 B
1 N
1 F
1 B
1 N
1 F
1 B
1 N
1 F
Flare Importance
19
20
21
22
23
24
25
26
27
28
29
30
Day